Sullo, N., Peloni, A., and Ceriotti, M. (2016) From Low Thrust to Solar Sailing: A Homotopic Approach. In: 26th AAS/AIAA Space Flight Mechanics Meeting, Napa, CA, USA, 14-18 Feb 2016, pp. 435-454.

There may be differences between this version and the published version. You are advised to consult the publisher's version if you wish to cite from it.

http://eprints.gla.ac.uk/124506/

Deposited on: 05 October 2016

FROM LOW THRUST TO SOLAR SAILING: A HOMOTOPIC APPROACH

N. Sullo,[*] A. Peloni,[*] and M. Ceriotti[†]

This paper describes a novel method to solve solar-sail minimum-time-of-flight optimal control problems starting from a low-thrust solution. The method is based on a homotopic continuation. This technique allows to link the low-thrust with the solar-sail acceleration, so that the solar-sail solution can be computed starting from the usually easier low-thrust one by means of a numerical iterative approach. Earth-to-Mars transfers have been studied in order to validate the proposed method. A comparison is presented with a conventional solution approach, based on the use of a genetic algorithm. The results show that the novel technique has advantages, in terms of accuracy of the solution and computational time.

INTRODUCTION

Low-thrust propulsion, such as the one produced by an electric thruster, is currently one of the most promising propulsion systems for interplanetary missions. On the other hand, solar sailing is an appealing technology, for being propellant-less. In general, for the design of both low-thrust and solar-sail trajectories, since no analytical solutions exist, an optimal control problem (OCP) must be solved numerically.[1,2] However, a solar sail cannot thrust towards the Sun and the magnitude of its acceleration is strictly related to the thrust direction and the distance from the Sun. On the other hand, low-thrust propulsion, at least in a preliminary design phase, does not usually have such constraints.[3] Thus, due to its constraints the solar-sail OCP is characterized by a more restricted space of feasible solutions with respect to the low-thrust one. That is, the solar-sail OCP becomes usually more difficult to solve numerically respect to a classical low-thrust one.

An approach very often used to solve space-transfers optimal problems consists in the use of the indirect method which is based on the Pontryagin Minimum Principle (PMP) formulation.[4] In this paper, the PMP formulation (also referred as Hamiltonian formulation) has been considered. Techniques adopted in the literature to solve space transfer OCPs via the Hamiltonian formulation usually make use of heuristic solvers.[5,6]

The aim of this work is to develop an efficient method to compute a solution for the solar-sail minimum-time-of-flight OCP, starting from a low-thrust solution of a similar transfer, which is easier to find. The efficiency of the proposed method regards both the computational time needed to get the solution and the level of accuracy of the solution itself.

---

[*] Ph.D. Candidate, School of Engineering, University of Glasgow, Glasgow G12 8QQ - United Kingdom.
[†] Lecturer in Space Systems Engineering, School of Engineering, University of Glasgow, Glasgow G12 8QQ - United Kingdom.

The method proposed makes use of the homotopy theory associated to numerical continuation:[7-9] the purpose is to properly link the low-thrust to the solar-sail minimum time-of-flight problem by means of a homotopy function. Consequently, it is possible to pass from the solution of the former OCP to the one of the latter OCP via the continuation method. The homotopy-continuation approach as already been adequately applied in literature to solve trajectory optimization problems, as shown in works carried out to find fuel-optimal low-thrust transfer trajectories.[10,11] In the current paper the authors reintroduce and properly adapt the above mentioned method, to serve as a competitive alternative respect to the conventional approaches to numerically solve solar-sail optimal problems.

The paper is organized as follows. In the first section the mathematical model is explained in detail. The second section shows the numerical test cases examined to validate and compare the approach proposed in the paper to the conventional heuristic-based methods used to find solar-sail optimal solutions. Further analysis are presented in the fourth and fifth section. In particular, in fourth section the results of a further investigation demonstrated that branches of solutions exist – for the solar-sail OCP – when performing the numerical continuation. Lastly, in the fifth section it is shown how it is possible to compute a solar-sail planet-rendezvous optimal transfer by means of numerical continuation and for any initial phase displacement between the departing and arriving planet. Conclusions and final remarks are drawn in the last section.

MATHEMATICAL MODEL

The basis of the proposed approach consists in the introduction of a homotopy function that continuously links the low-thrust to the solar-sail optimal problem. Next, the numerical continuation, by means of an iterative approach, allows computing the solution of the final solar sail OCP starting from the solution of the easier low-thrust OCP, which is already known or can be obtained without a particular effort. Two-dimensional two-body dynamical system has been considered. Within the dynamic model taken into account, the homotopic transformation (as described later in this section) is introduced on the acceleration that is provided by the spacecraft. Thereby the spacecraft acceleration can be continuously transformed (by continuation) from the one provided by a low-thrust system to the one given by a sailcraft.

The low-thrust acceleration is defined according to the expression

$$\boldsymbol{a}_{LT} = a_{\max} u \begin{bmatrix} \cos \alpha \\ \sin \alpha \end{bmatrix} \tag{1}$$

where $a_{\max}$ and $u_{LT} \in [0,1]$ are respectively referred to the low-thrust maximum acceleration and non-dimensional control. It is necessary to remark that the spacecraft mass variation is not considered in the dynamic equations. This because the optimal-control law for a low-thrust propelled spacecraft is transformed to the one for a sailcraft that is characterized by being propellant-less. The solar-sail is modeled as ideal and perfectly-reflecting sail, for which the acceleration provided is defined according to the expression

$$\boldsymbol{a}_{SS} = a_c \left(\frac{r_\oplus}{r} \right)^2 \cos^2 \alpha \begin{bmatrix} \cos \alpha \\ \sin \alpha \end{bmatrix} \tag{2}$$

where a_C is the solar-sail characteristic acceleration, $r_\oplus$ the mean Earth distance from the Sun, r and α respectively the sail radial position and cone angle, i.e. the angle between the radial direction $\hat{\boldsymbol{u}} = \dfrac{\boldsymbol{u}}{\|\boldsymbol{u}\|}$ and the thrust direction $\hat{\boldsymbol{n}}$ (see Figure 1). Circular and planar Earth and Mars

orbits have been considered for the space transfers examined (Earth radius $R_E = 1\,\text{AU}$, Mars radius $R_M = 1.52368\,\text{AU}$).[12]

Coordinates system and reference frame

A polar coordinate system is used in the transcription of the optimal control problem. The coordinate system as well as the reference frame – considered Sun centered – is represented in Figure 1. The state vector takes the form:

$$x = \begin{bmatrix} r & \vartheta & u & v \end{bmatrix}^T \tag{3}$$

where r is the radial distance of the spacecraft measured from the Sun, ϑ identifies the spacecraft angular position respect to a fixed axis in the space (inertial), u and v are respectively the radial and transversal spacecraft velocities.
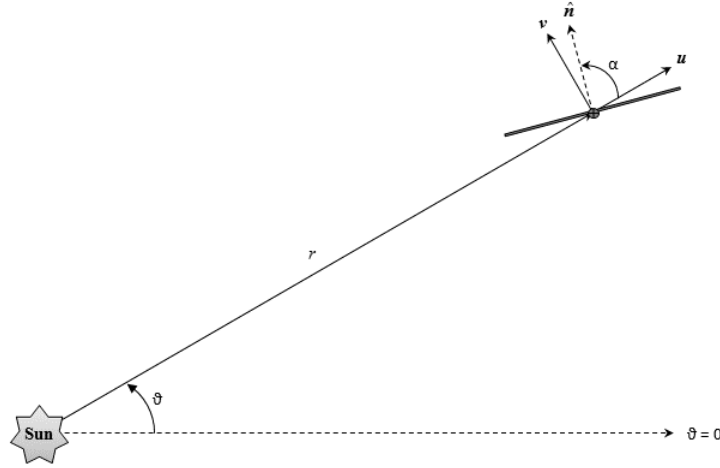

Figure 1. Reference frame and state variables.

Dynamic equations

This sub-section describes the dynamic equations for both low-thrust and solar-sail spacecraft and the OCP conditions.

Low thrust. The dynamics of a generic low-thrust propelled spacecraft is modeled as follows:

$$\dot{x} = f_g + f_{a,LT} = \begin{bmatrix} u \\ \dfrac{v}{r} \\ \dfrac{v^2}{r} - \dfrac{\mu}{r^2} \\ -\dfrac{uv}{r} \end{bmatrix} + a_{max} u_{LT} \begin{bmatrix} 0 \\ 0 \\ \cos\alpha \\ \sin\alpha \end{bmatrix}, \quad \alpha \in [-\pi, \pi] \tag{4}$$

where f_g identifies the contribution to the state equations due to the Sun's gravitational attraction, $f_{a,LT}$ identifies instead the contribution due to the acceleration provided by the thruster, as in Eq. (1). μ refers to the Sun's gravitational parameter.

3

Solar sail. The dynamical equations, for an ideal solar sail, are defined as follows:[12]

$$\dot{\boldsymbol{x}} = \boldsymbol{f}_g + \boldsymbol{f}_{a,SS} = \begin{bmatrix} u \\ \dfrac{v}{r} \\ \dfrac{v^2}{r} - \dfrac{\mu}{r^2} \\ -\dfrac{uv}{r} \end{bmatrix} + a_C \left(\dfrac{r_\oplus}{r} \right)^2 \cos^2 \alpha \begin{bmatrix} 0 \\ 0 \\ \cos \alpha \\ \sin \alpha \end{bmatrix} \tag{5}$$

where $\boldsymbol{f}_{a,SS}$ is the acceleration contribution due to the solar sail, as defined in Eq. (2). It is note-worthy to remind that for an ideal solar sail the acceleration provided is always directed perpendicularly to the sail surface and it always has its radial component greater than or equal to zero; to achieve this, the cone angle is constrained to $\alpha \in \left[-\dfrac{\pi}{2}, \dfrac{\pi}{2} \right]$.

Optimal control problem formulation

The PMP conditions are now introduced for both the low-thrust and solar-sail minimum time of flight problem.[2] These formulations are subsequently used to introduce and describe the homotopy-continuation method, focus of the current study.

The problem cost function, common for both low-thrust and solar-sail OCPs, is the total time of flight for the transfer trajectory

$$J = t_{0f} = t_f - t_0 \tag{6}$$

where t indicates the time and subscripts 0 and f refer to the initial and final times respectively.

The Hamiltonian is given by

$$H = \boldsymbol{\lambda}^T \dot{\boldsymbol{x}} \tag{7}$$

where the vector of costates is defined as $\boldsymbol{\lambda} = \begin{bmatrix} \lambda_r & \lambda_g & \lambda_u & \lambda_v \end{bmatrix}^T$.

The PMP conditions – derived by the minimization of the Hamiltonian – state that the costate equations are defined by

$$\dot{\boldsymbol{\lambda}} = -\dfrac{\partial H}{\partial \boldsymbol{x}} \tag{8}$$

and the optimal control law by

$$\alpha = \underset{\alpha \in U}{\operatorname{argmin}} H \tag{9}$$

where U is the subset of existence of feasible solutions for the optimal problem considered.

Eq. (9) can be rewritten in a more straightforward form as

$$\tan \alpha = \left(\dfrac{\lambda_v}{\lambda_u} \right) \tag{10}$$

and $u_{LT} = 1$ for a low-thrust system, and for a sailcraft:[13]

4

$$\tan\alpha = \left(\frac{-3\lambda_u - \sqrt{9\lambda_u^2 + 8\lambda_v^2}}{4\lambda_v} \right) \tag{11}$$

Furthermore, according to the optimality conditions, the following boundary conditions shall be satisfied in the case of an orbit transfer

$$\boldsymbol{\psi}_0 = \begin{bmatrix} r(t_0) - r_0 \\ \vartheta(t_0) - \vartheta_0 \\ u(t_0) - u_0 \\ v(t_0) - v_0 \end{bmatrix} = \mathbf{0} \ , \ \boldsymbol{\psi}_f = \begin{bmatrix} r(t_f) - r_f \\ u(t_f) - u_f \\ v(t_f) - v_f \end{bmatrix} = \mathbf{0} \ , \ \boldsymbol{\psi}_{tr} = \begin{bmatrix} \lambda_\vartheta(t_f) \\ H(t_f) + 1 \end{bmatrix} = \mathbf{0} \tag{12}$$

In the case of a planet rendezvous, the boundary conditions to be satisfied are as follows

$$\boldsymbol{\psi}_0 = \begin{bmatrix} r(t_0) - r_0 \\ \vartheta(t_0) - \vartheta_0 \\ u(t_0) - u_0 \\ v(t_0) - v_0 \end{bmatrix} = \mathbf{0} \ , \ \boldsymbol{\psi}_f = \begin{bmatrix} r(t_f) - r_f \\ \vartheta(t_f) - \vartheta_f \\ u(t_f) - u_f \\ v(t_f) - v_f \end{bmatrix} = \mathbf{0} \ , \ \psi_{tr} = H(t_f) - \omega_M \lambda_\vartheta(t_f) + 1 = 0 \tag{13}$$

where ω_M is the constant angular velocity of the Mars orbit.

HOMOTOPIC SOLUTION APPROACH

The homotopy can be defined as a function linking continuously two continuous functions from a topological space X to another Y (see Reference 7).

The functions to be linked by the homotopy are the shooting functions relative to the low-thrust and solar-sail OCPs, respectively. The shooting function is represented by a nonlinear function given by $\Phi(z) : \mathbb{R}^n \to \mathbb{R}^m$, where n is the number of optimization variables of the OCP, while m is the number of nonlinear equations provided by the boundary conditions at the final time for the OCP at hand (see Eq. (12) and Eq. (13))[10,11]

$$\Phi(z) = \begin{bmatrix} \boldsymbol{\psi}_0 & \boldsymbol{\psi}_f & \boldsymbol{\psi}_{tr} \end{bmatrix}^T \tag{14}$$

z represents the vector of the optimization variables given by the initial values of the costates λ_0 and the time of flight

$$z = \begin{bmatrix} \lambda_0 & t_{0f} \end{bmatrix}^T \tag{15}$$

The zeroes of the shooting function represent the solution to the optimal problem. Thence, the homotopy becomes defined by the nonlinear function $\Phi(z,\varepsilon) : \mathbb{R}^n \times \mathbb{R} \to \mathbb{R}^m$, where ε is the so-called homotopic-transformation parameter, belonging to the interval $\varepsilon \in [0,1]$. When $\varepsilon = 0$ the homotopy becomes the shooting function relative to the low-thrust optimal problem, when instead $\varepsilon = 1$ the homotopy turns into the shooting function relative to the solar-sail optimal problem.

Homotopy transformation

The homotopy transformation that makes possible to link the low-thrust to the solar-sail OCP is now introduced on the spacecraft acceleration formulation.

A linear homotopic transformation on the spacecraft acceleration is introduced as:

$$\boldsymbol{a}_{LTSS} = a_{\max}\left[(1-\varepsilon)u + \left(\left(\frac{r_{\oplus}}{r}\right)^2 \cos^2\alpha\right)\varepsilon\right]\cdot\begin{bmatrix}\cos\alpha\\\sin\alpha\end{bmatrix} \tag{16}$$

with $\alpha \in [-\pi,\pi]$ and ε the homotopic-transformation parameter. The corresponding homotopy is

$$\boldsymbol{\Phi}(z,\varepsilon) = \boldsymbol{0} \tag{17}$$

The relation in Eq. (16) links the low-thrust acceleration of Eq. (1) to the one that can be provided by a "pseudo solar sail", provided by Eq. (2) with $a_c = a_{\max}$ and no constraints on the thrust direction (or cone angle α).

The solution of $\boldsymbol{\Phi}(z,1) = \boldsymbol{0}$, for which $\alpha \in [-\pi,\pi]$, is used as initial guess for the computation of the real solar-sail OCP through a single-shooting approach. This consists in the computation of the zeroes of $\boldsymbol{\Phi}(z,1) = \boldsymbol{0}$ subject to the constraint $\alpha \in \left[-\dfrac{\pi}{2},\dfrac{\pi}{2}\right]$.

If the desired characteristic acceleration is different with respect to the corresponding low-thrust acceleration (i.e. $a_c \neq a_{\max}$), the homotopy-continuation technique can be applied again as explained below. A second homotopy transformation on the characteristic acceleration is introduced, in order to link the starting solar-sail solution with $a_c = a_{c,0} = a_{\max}$ to the final one having $a_c = a_{c,f} \neq a_{\max}$:

$$\boldsymbol{a}'_{SS} = \left[(1-\varepsilon')a_{c,0} + \varepsilon'a_{c,f}\right]\left(\left(\frac{r_{\oplus}}{r}\right)^2 \cos^2\alpha\right)\cdot\begin{bmatrix}\cos\alpha\\\sin\alpha\end{bmatrix} \tag{18}$$

In this case, the corresponding homotopy is given by

$$\boldsymbol{\Phi}'(z,\varepsilon') = \boldsymbol{0} \tag{19}$$

As already discussed, numerical continuation is used to continue and follow the solutions of the homotopy until finally compute the desired solar-sail solution.

Transformed optimal control problem formulation

The formulation of the PMP conditions for the minimum time-of-flight problem becomes more complex, when the homotopy transformation on the spacecraft acceleration in Eq. (16) is included. Therefore, it is necessary to provide a clear explanation of how the optimality conditions are retrieved.

The main differences respect to the PMP conditions derived earlier relate to the dynamic equation and the optimal control law. The dynamics is now described by

$$\dot{\boldsymbol{x}} = \boldsymbol{f}_g + \boldsymbol{f}_{a,LTSS} = \begin{bmatrix} u \\ \dfrac{v}{r} \\ \dfrac{v^2}{r} - \dfrac{\mu}{r^2} \\ -\dfrac{uv}{r} \end{bmatrix} + a_{\max}\left[(1-\varepsilon)u_{LT} + \left(\left(\frac{r_{\oplus}}{r}\right)^2 \cos^2\alpha\right)\varepsilon\right]\begin{bmatrix} 0 \\ 0 \\ \cos\alpha \\ \sin\alpha \end{bmatrix} \tag{20}$$

The expanded expression of the Hamiltonian system derived after some algebra is

$$H = \boldsymbol{\lambda}^T \dot{\boldsymbol{x}} = H_1 + H_2$$
$$H_1 = \boldsymbol{\lambda}^T \boldsymbol{f}_g \tag{21}$$
$$H_2 = \boldsymbol{\lambda}^T \boldsymbol{f}_{a,LTSS} = A\sin(\alpha) + B\cos(\alpha) + C\cos^3(\alpha) + D\sin(\alpha)\cos^2(\alpha)$$

where the multipliers coefficients in H_2 are given by

$$A = \lambda_v \left((1-\varepsilon)u_{LT}a_{max}\right) , \quad B = \lambda_u \left((1-\varepsilon)u_{LT}a_{max}\right)$$
$$C = \lambda_u \left(\varepsilon a_{max}\left(\frac{r_\oplus}{r}\right)^2\right) , \quad D = \lambda_v \left(\varepsilon a_{max}\left(\frac{r_\oplus}{r}\right)^2\right) \tag{22}$$

The PMP conditions derived by the Hamiltonian minimization lead to different relations only with regard to the optimal control law. The variables relative to the optimal control are identified by the low-thrust non-dimensional control u_{LT} and the control angle α. By equating to zero the partial derivatives of the Hamiltonian with respect to the above-mentioned variables, it results:

$$\frac{\partial H}{\partial u_{LT}} = (1-\varepsilon)a_{max}u_{LT}(\lambda_u\cos(\alpha) + \lambda_v\sin(\alpha)) = 0 \tag{23}$$

$$\frac{\partial H}{\partial \alpha} = (A+D)\tau^6 + 2(B+3C)\tau^5 + (A-11D)\tau^4 + 4(B-3C)\tau^3 - (A-11D)\tau^2 + 2(B+3C)\tau - (A+D) = 0 \tag{24}$$

where $\tau = \tan\left(\dfrac{\alpha}{2}\right)$, thus $\alpha = 2\tan^{-1}(\tau)$.

From Eq. (23) the optimal law for the non-dimensional control is retrieved as

$$\begin{cases} u_{LT} = 1 & if \ (\lambda_u\cos(\alpha) + \lambda_v\sin(\alpha)) < 0 \\ u_{LT} = 0 & if \ (\lambda_u\cos(\alpha) + \lambda_v\sin(\alpha)) > 0 \end{cases} \tag{25}$$

while from Eq. (24) the values for the control angle α are obtained by numerically finding the roots of the sixth order polynomial expression. Although an analytical expression can be found for only two roots of the polynomial, the remaining roots of the fourth order polynomial resulting after factorization can be only found numerically. Since no actual improvement (in terms of computational speed) results from the polynomial factorization, the roots of the sixth order polynomial are all computed numerically.

However, the optimal control variables u_{LT} and α appear in both Eq. (23) and Eq. (24) and are nonlinearly dependent on each other. Also, since more than one optimal solution exist, the optimal values of u_{LT} and α are those that minimize the Hamiltonian. The strategy adopted consists in computing for $u_{LT} = \{0,1\}$ the real roots of the polynomial expression of Eq. (24) and then retrieving the value of α and the corresponding value of u_{LT} that minimize the Hamiltonian.

Transversality condition avoidance

It is important to note that the costate differential equations for the transformed optimal problem are homogenous. The particular structure of these equations can be clearly highlighted providing their explicit formulation:

$$\dot{\lambda}_r = \lambda_u \left(\frac{v^2}{r^2} - \frac{2\mu}{r^3} + \frac{2\varepsilon a_c r_\oplus^2 \cos^3 \alpha}{r^3} \right) - \lambda_v \left(\frac{uv}{r^2} - \frac{2\varepsilon a_c r_\oplus^2 \cos^2 \alpha \sin \alpha}{r^3} \right) + \lambda_\vartheta \left(\frac{v}{r^2} \right)$$

$$\dot{\lambda}_\vartheta = 0$$

$$\dot{\lambda}_u = -\lambda_r + \lambda_v \left(\frac{v}{r} \right)$$

$$\dot{\lambda}_v = -\lambda_\vartheta \left(\frac{1}{r} \right) + \lambda_v \left(\frac{u}{r} \right) - \lambda_u \left(\frac{2v}{r} \right)$$

(26)

If an optimization algorithm is able to find initial values for the costates that are scaled respect to the optimal ones

$$\boldsymbol{\lambda}(0) = a\boldsymbol{\lambda}^*(0) \ , \ a \in \mathbb{R}^+$$

(27)

then the proportionality relation in Eq. (27) holds at any time t due to the homogeneity of Eq. (26). Furthermore, if scaled costates are considered, the PMP conditions provided by Eq. (23) and Eq. (24) remain unchanged. Thus implies that also the optimal control law for the trans-formed OCP remains unchanged and consequently the optimal state variables remain unaffected. Therefore the boundary conditions provided in Eq. (12) or in Eq. (13) remain satisfied, except for the Hamiltonian conditions that become for the orbit transfer:

$$H(t_f) = -a$$

(28)

and for the planet rendezvous problem:

$$H(t_f) - \omega_M \lambda_\vartheta(t_f) = -a$$

(29)

Hence it results that the transversality condition on the Hamiltonian is ignorable and can be neglected in the minimum-time-of-flight OCP formulation. Indeed, equality constraints (such as the Hamiltonian condition) can "narrow considerably the search space in which feasible solutions can be located".[5,6] By adopting the aforementioned constraint reduction, a simplification of the optimal solution computation can be achieved for heuristic solvers. This is generally true also for deterministic solvers, since at least a lower number of numerical calculations is involved. For these reasons and for a matter of consistency the Hamiltonian transversality condition has been neglected in all the numerical test cases computed in the current study (for both the heuristic and deterministic solvers used).

It is worth noting that – since one fewer condition is considered – the nonlinear system to be solved (given by Eq. (12) or Eq. (13) without the Hamiltonian condition) becomes rectangular, i.e. the number of nonlinear equations is less than the number of the unknowns. In order to deal with the solution of a rectangular nonlinear system, the Levenberg-Marquardt solver has been used in the numerical continuation.[14] The use of this algorithm has proved to be adequate to compute final solutions that satisfy – inside the preset tolerances – all the necessary PMP conditions.

Numerical continuation

The use of numerical continuation allows computing the solution of the final OCP – the ze-roes of the solar-sail shooting function – starting from the solution of the easier OCP, i.e. the ze-roes of the low-thrust shooting function. In fact, this technique makes it possible to follow the so-called "zero-path" of the homotopy (i.e. the locus of solutions (z^*, ε^*) of the system $\boldsymbol{\Phi}(z, \varepsilon) = \boldsymbol{0}$) by continuing the parameter ε, starting from the solution relative to $\varepsilon = 0$ until computing the final desired solution at $\varepsilon = 1$. The numerical continuation algorithm adopted in the current work

8

has been implemented in the form of discrete continuation.[10,11] It consists in progressively increasing the value of the homotopic-transformation parameter ε and, for each step, computing the solution of an intermediate OCP. Each intermediate solution is used as a starting point for the computation of the following intermediate OCP, until finally reaching the desired solution. The continuation step size is adaptively determined. If convergence is achieved at an intermediate iteration, the algorithm doubles the step size to speed up the continuation process. If no convergence is achieved, the step size is halved and the continuation iteration is run again with a decreased step size, until convergence is reached. However, there can be cases in which the continuation process does not converge: the step size continues to be halved until reaching its preset minimum value and therefore the algorithm terminates. In fact, the discrete continuation – since it does not consist in a real zero-path following algorithm – can fail especially in cases where the zero-path is not smooth enough or presents folds. In most of the numerical analysis performed and in the test cases –presented in the following, the homotopic zero-path has proved to be adequately smooth and regular, so that the discrete-continuation algorithm demonstrated to be robust enough to converge. However, there are cases in which the convergence of the discrete continuation is numerically influenced by an appropriate choice of the parameters involved in the continuation algorithm. An investigation regarding the possibility of fold occurrence in the homotopic zero-paths has not been undertaken yet.

NUMERICAL TEST CASES

In order to compare the performance of the novel approach with a traditional one, several comparative tests are presented and analyzed. Within the same Hamiltonian formulation, the solar-sail optimal control problem is solved by means of homotopy, and through a conventional evolutionary approach. Four test cases have been considered (Table 1) for the purpose to (a) validate the novel method proposed for computing solar-sail OCPs and (b) compare its performance with respect to a conventional genetic algorithm (GA) method used to solve the same solar-sail OCPs.

Table 1. Numerical test cases

	$a_c \,[\mathrm{mm/s^2}]$	Type of transfer
Test case 1	1	Orbit transfer
Test case 2	0.1	Orbit transfer
Test case 3	1	Planet rendezvous
Test case 4	0.1	Planet rendezvous

The GA is used to solve the solar sail OCPs by giving as objective function to minimize the ℓ^2-norm of the shooting function ($\left\|\Phi(z,1)\right\|$ or $\left\|\Phi'(z,1)\right\|$, according to the specific test case).

In order to have a comprehensive comparison, 20 different sets of settings have been considered for the GA simulations, by changing the population size ($Population = \{50,100,150,200,500\}$) and the maximum number of generations allowed ($MaxGenerations = \{500,1000,1500,2000\}$). Because of the heuristic nature of the GA, each set of settings has been run 100 times and statistical values have been taken into account for the comparison.

The tolerances on the final position and velocity have been set to 1000 km for the position error and 0.1 m/s for both the radial and transversal velocity errors, as stated in the reference paper.[12] These tolerances are the same for all the test cases taken into account in this work. It is also

worth mentioning that a C++ implementation of the Bulirsch-Stoer algorithm has been used to more efficiently propagate the dynamics equations, with higher accuracy and lower computational effort respect to the conventional ODE solvers.[15] The absolute and relative tolerances for the propagator have both been set to 10^{-8} (see Reference 12). All the simulations have been performed in MATLAB on a 3.4 GHz Core i7-3770 with 16 GB of RAM, running Linux Ubuntu 14.04.

Test case 1

The first test case is the planar circular-to-circular Earth-Mars orbit transfer.[12] The low-thrust maximum acceleration has been considered the same as the characteristic acceleration: $a_{\max} = a_c = 1 \text{ mm/s}^2$. The results of both the homotopy approach and the GA are shown in Table 2. The results for GA are expressed in terms of success rate of each set of setting, i.e. the percentage of runs (out of 100) which terminate with at least one feasible solution (a solution within the required tolerances). The first row of Table 2 shows the number of sets with a success rate above 90%. It is important to underline that the homotopy is a deterministic approach, so it can be either successful or not successful. Table 2 shows that the result obtained through the homotopy approach is consistent with the ones obtained via the GA method. Moreover, the result presented in Reference 12 ($t_{0f} = 407.7 \text{ days}$) is in perfect agreement with the results shown in Table 2. Only 8 sets of settings of the GA out of 20 have a success rate above 90% and the homotopy method is 42% faster than the GA. The computational time shown in the GA column of Table 2 represents the lowest average computational time among all the sets of settings with a success rate above 90%.

Table 2. Test case 1: homotopy and GA results comparison

	Homotopy	GA
Sets with success rate above 90%	-	8 out of 20
Computational time [s]	11	19
t_{0f} [days]	407.72	$[407.69, \ 407.72]$

Figure 2a shows the control evolution during the first continuation – low thrust to pseudo solar sail as described in Eq. (16) – while Figure 2b shows the comparison between the control of the low-thrust and the one of the solar sail. Figure 3a and Figure 3b show the low-thrust and solar-sail transfer trajectories, respectively. A plot of the acceleration vector along the transfer is also shown.
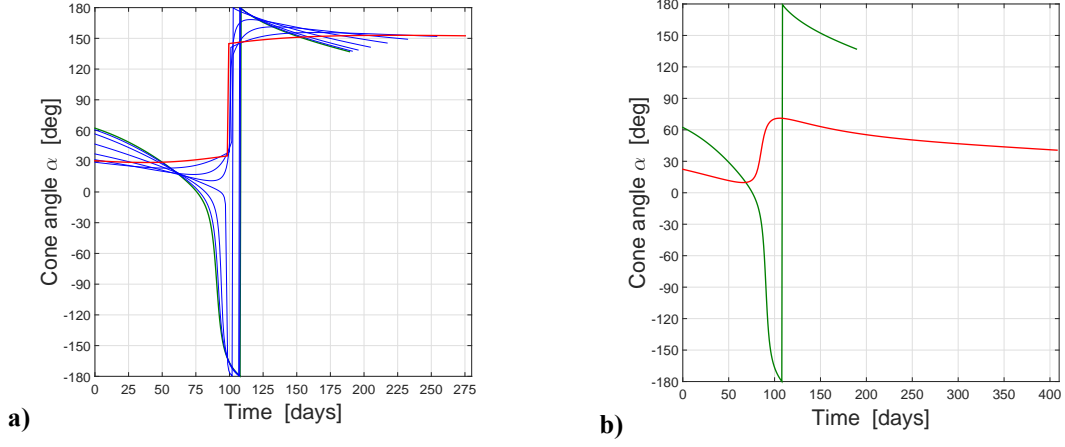
10

Figure 2. Test case 1, cone angle evolution over time during the 1ˢᵗ continuation. (a) The green line represents the low-thrust cone angle, the red line the pseudo solar-sail one, while the blue lines show the evolution of the cone angle during the continuation. (b) The green line represents the low-thrust cone angle, while the red line is the solar sail one.
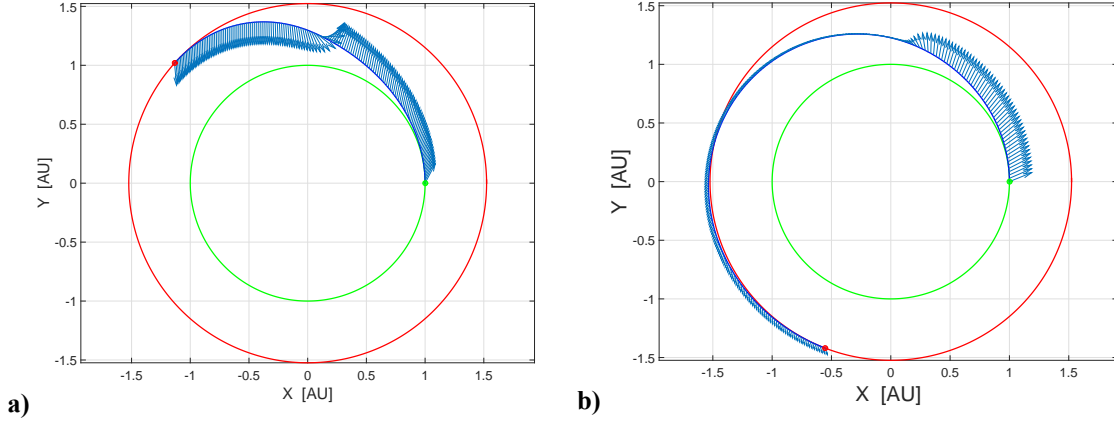

Figure 3. Test case 1, transfer trajectories. (a) Low-thrust. (b) Solar-sail.

Test case 2

A second scenario has been tested, considering the same problem, but with a smaller solar-sail characteristic acceleration ($a_c = 0.1$ mm/s²). This means that the second continuation described in Eq. (18) can be applied to the solution of the previous test case. On the other hand, the optimizations through GA shall be repeated with the new value of the characteristic acceleration. Table 3 shows the comparison between the results of the homotopy approach and GA.

11

Table 3. Test case 2: homotopy and GA results comparison

	Homotopy	GA
Sets with success rate above 90%	-	14 out of 20
Computational time [s]	12	16
t_{0f} [days]	2661.51	$[2661.34,\ 2661.43]$

Figure 4a shows the evolution of the cone angle during the second continuation, where the characteristic acceleration changes from $a_{c,0} = 1\ \text{mm/s}^2$ to $a_{c,f} = 0.1\ \text{mm/s}^2$. Figure 4b shows the planar circular-to-circular Earth-Mars transfer trajectory through a solar sail with $a_c = 0.1\ \text{mm/s}^2$.
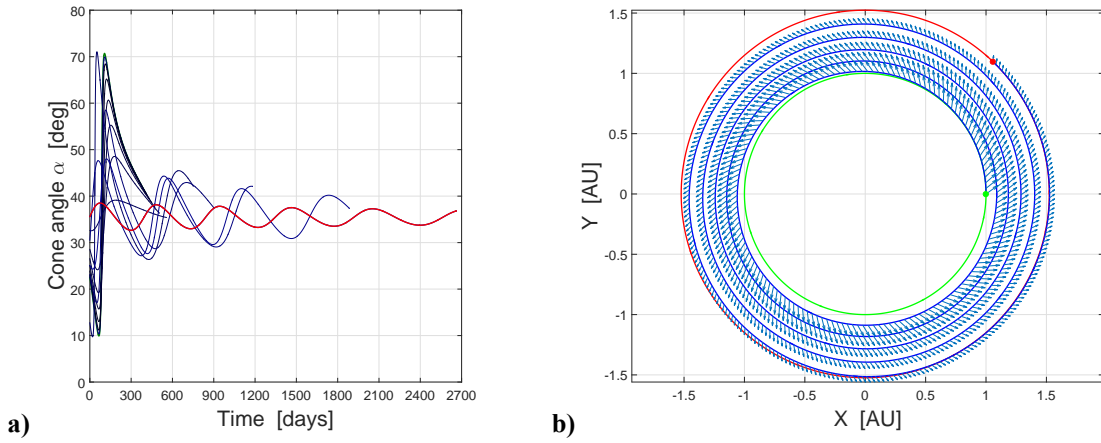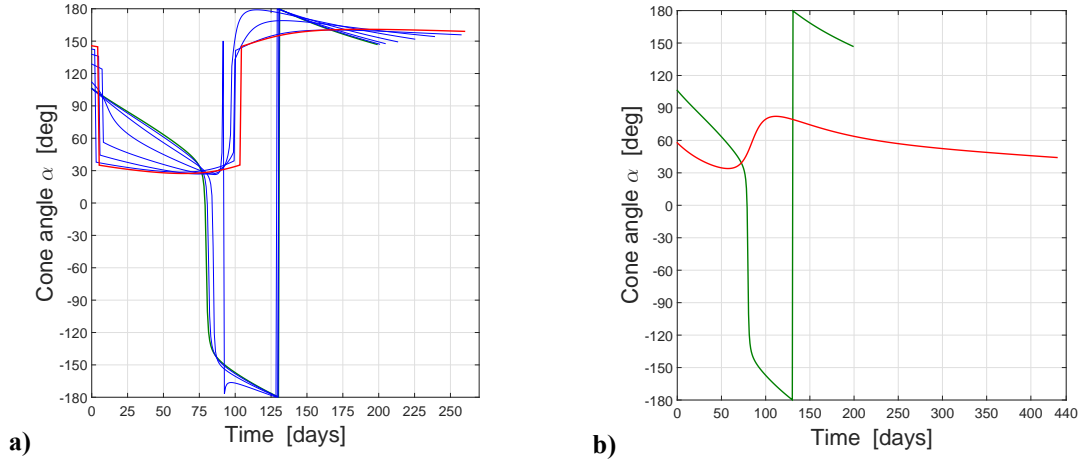

Figure 4. Test case 2. (a) Cone-angle evolution during the 2nd continuation: the green line represents the low-thrust cone angle, the red line the pseudo solar-sail one, while the blue lines show the evolution of the cone angle during the continuation. (b) Solar-sail transfer trajectory.

Test case 3

Test cases 3 and 4 aim to demonstrate the performance of the proposed method on a planetary rendezvous. Therefore, within the same planar circular-to-circular Earth-Mars scenario, a planetary rendezvous with Mars has been set, where the positions of the planets are found using analytical ephemerides. This results in a considerably more difficult problem, since the final angular position is constrained and the constraint is a function of time. In fact, the final boundary constraint on ϑ depends on the time of flight, which in turn is also the objective function of the OCP. In both test cases, the launch date has been fixed to February, 14th 2016, when the initial Earth-Mars phase displacement is $\varphi = 49.3\ \text{deg}$.

Table 4 shows the results obtained for the third test case, by considering $a_c = 1\ \text{mm/s}^2$. Since this problem appears to be more difficult to solve for the GA (within the required tolerances), the solutions from GA have been refined by means of a gradient-based method, which is implemented in the "interior-point" algorithm in the MATLAB function *fmincon*. It is worth to underline that, even if the gradient-based method has been used to help GA, the success rates among all the sets of settings considered are below 40%. In this case, the computational-time record of

GA in Table 4 refers to the minimum one among all the sets of parameters with a success rate above 30%.

Table 4. Test case 3: homotopy and GA results

	Homotopy	GA
Sets with success rate above 30%	-	5 out of 20
Computational time [s]	27	27
t_{0f} [days]	429.58	$[429.57, \ 429.59]$

Figure 5a shows the control evolution during the first continuation, as described in Eq. (16), while Figure 5b shows the comparison between the control evolutions of the low-thrust and the one of the solar sail.

a)

b)

Figure 5. Test case 3, cone angle evolution during the 1st continuation. (a) The green line represents the low-thrust cone angle, the red line the pseudo solar-sail one, while the blue lines show the evolution of the cone angle during the continuation. (b) The green line represents the low-thrust cone angle, while the red line is the solar-sail one.
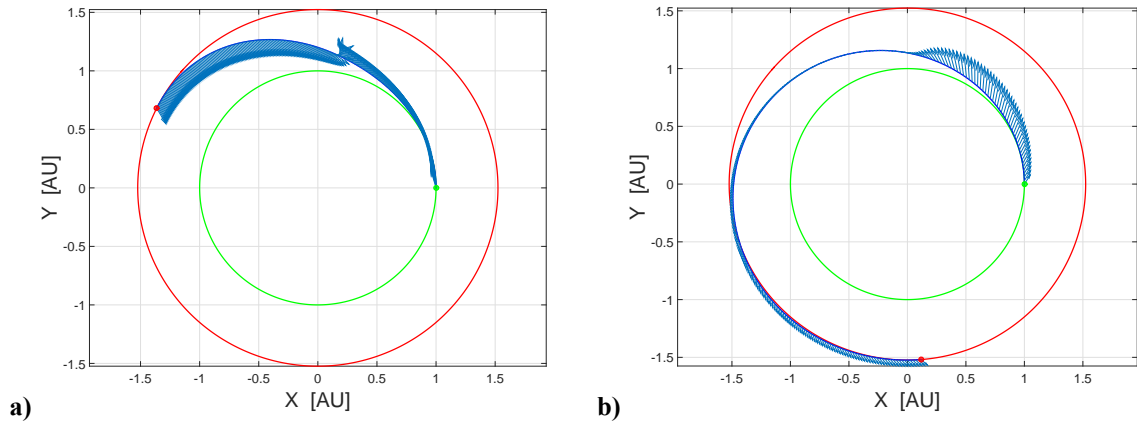

a)

b)

Figure 6. Test case 3, transfer trajectories. (a) Low-thrust. (b) Solar-sail.

Test case 4

Test case 4 is the planar circular-to-circular Earth-Mars rendezvous through a solar sail with $a_c = 0.1 \text{ mm/s}^2$. The GA has been used only with one set of settings (Population = 500, MaxGenerations = 10000). The results are shown in Table 5.

Table 5. Test case 4: homotopy and GA results

	Homotopy	GA
Success rate (over 100 runs)	-	20%
Computational time [s]	36	1219
t_{0f} [days]	3773.93	3773.23

Figure 7 shows the evolution of the cone angle during the second continuation, Eq. (18), where the characteristic acceleration changes from $a_{c,0} = 1 \text{ mm/s}^2$ to $a_{c,f} = 0.1 \text{ mm/s}^2$. Figure 7 shows the planar circular-to-circular Earth-Mars rendezvous trajectory through a solar sail with $a_c = 0.1 \text{ mm/s}^2$.
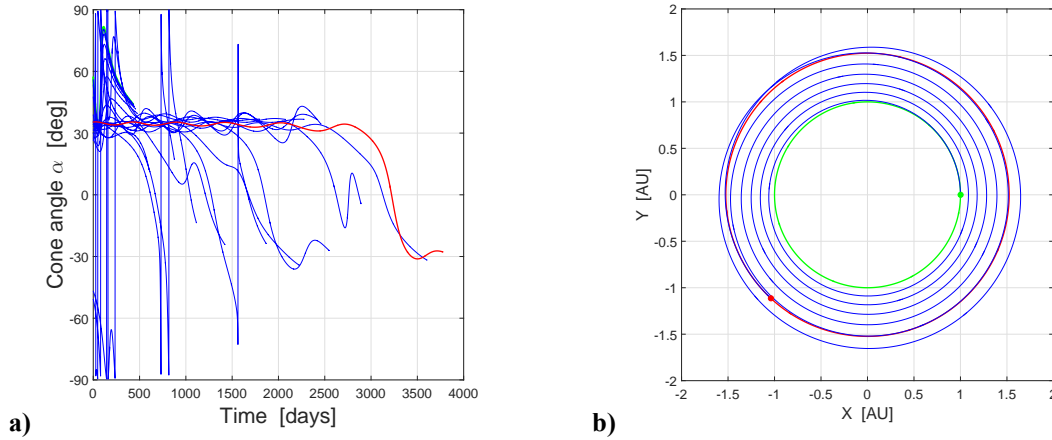

a)   b)

Figure 7. Test case 4. (a) Cone angle evolution during the 2nd continuation: the green line represents the low-thrust cone angle, the red line the pseudo solar-sail one, while the blue lines show the evolution of the cone angle during the continuation. (b) Solar-sail transfer trajectory.

As demonstrated in the four test cases, the homotopy method shows good performance in dealing with solar-sail trajectories. Given a low-thrust trajectory, in fact, one is able to easily and quickly find a solar-sail optimal trajectory, while the genetic algorithm hardly finds solutions within the given tolerances. The results of the first three test cases show that the solutions found through the homotopy-continuation method are likely to be global-optimal solutions, since the time of flight is always comparable with the one found by the GA. Moreover, the method allows to have solar-sail solutions for a wide range of characteristic accelerations through the second continuation relative to Eq. (18). All the cone angles shown in Figure 4 and Figure 7, in fact, represent optimal solutions for $a_c \in [0.1, \ 1] \text{ mm/s}^2$.

14

ZERO-PATH BRANCHES AND MULTIPLE LOCAL MINIMA

In numerical continuation, the locus of solutions (z^*, ε^*) to a system $\Phi(z, \varepsilon) = \mathbf{0}$ generally consists of a branched-curves family. Each branch corresponds to a different dynamical behavior of the system depending on the continuation parameter. The branching points are called bifurcation points and they have specific mathematical definition, according to the specific type of bifurcation occurring.[16] In the specific case of study the zero-path is defined by the locus $(z^*, \varepsilon^*) = \left(\begin{bmatrix} \lambda_0^* & t_{0f}^* \end{bmatrix}^T, \varepsilon^* \right)$.

A deeper investigation described in this section focuses to study the zero-paths of the homotopies $\Phi(z, \varepsilon)$ and $\Phi'(z, \varepsilon')$ with the intent to understand if bifurcations occur. Recognizing bifurcations assumes an important role since branches in the zero-path lead to different local minima for the solar-sail OCP. Therefore, among these minima, the best solution in terms of time of flight can be chosen. The analysis here undertaken does not make use of specific tools designed to locate bifurcation points and continuing the branching solutions. However, a simple alteration of the algorithm performing the discrete continuation makes possible to identify multiple zero-path curves of the homotopies mentioned above. It shall be stressed that the approach used is not intended to be a methodology for studying bifurcations and continuing branching families. In addition, it is not expected that the branching curves found constitute all the possible existing branching solutions for the specific problem.

The modification to the discrete continuation algorithm consisted in an alteration of the values of the algorithm-parameters involved in determining the adaptive continuation step size. At each change of these parameters a full continuation – both on the first and second homotopy – has been carried out and the respective zero-path computed.

The initial costates and the time of flight have been used to describe the zero-paths of the homotopies. The initial costates represent mathematical entities necessary to determine the optimal control and thus the optimality of the solution. For a matter of concision in the exposition of the results and without missing information details, the $\ell^2 - \text{norm}$ of the initial costates is chosen to describe the behavior of the initial costate solutions resulting from continuation as function of the continuation parameter.[17] Therefore, two different behaviors can be described in the zero-paths of the first and second homotopy. In fact, the first continuation is characterized by different costate solutions, not bifurcating at any point, leading to the same optimal solution in terms of time of flight. In the second continuation, instead, different branching solutions of the initial costates lead to distinct branching solutions for the time of flight. Further explanations and evidences of these behaviors are given in the plots and comments below.

In this study, the first and second continuation relate to what shown in test case 3 and test case 4, respectively. Figure 8 shows the $\ell^2 - \text{norm}$ of the initial costate vector $\|\lambda_0\|$ and the time of flight t_{0f} both against the first continuation parameter ε. Although the continuation ends when $\varepsilon = 1$, the aforementioned plots show a further solution for $\varepsilon > 1$. This arrangement has been solely adopted to clearly show in the same plot the solution for a pseudo solar-sail transfer – at $\varepsilon = 1$, end of first continuation – and the one relative to the real solar-sail transfer, plotted at a certain $\varepsilon > 1$.
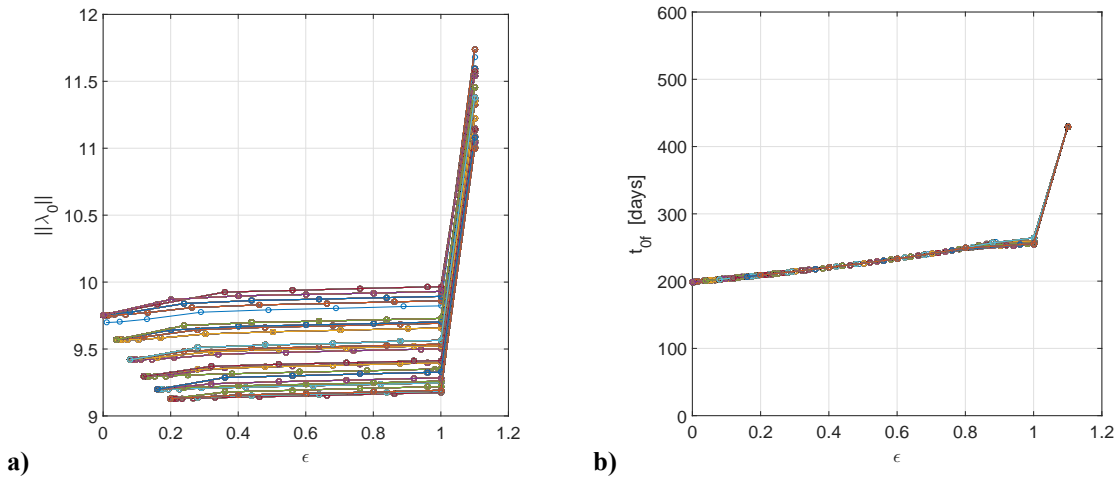
Figure 8. 1ˢᵗ continuation zero-path solutions. The pseudo-solar-sail solution corresponds at $\varepsilon = 1$, while the solar-sail solution is shown at $\varepsilon > 1$. The initial solutions shown start at different values of ε, depending on the first effective continuation step. In (a) the Euclidean norm of the initial costates and in (b) the time of flight are plotted as function of the continuation parameter.

Even though the initial costates show several distinct branches in the first continuation, the respective branches relative to the time of flight are almost all overlapping and all leading to the same final solution. The authors believe that this behavior is due in neglecting the transversality condition relative to the Hamiltonian. This implies that the same optimal solution can be computed for different values of the initial costates, which are only scaled with respect to each other, by a real and positive value.

A different behavior is instead exhibited by the zero-path branches in the second continuation, as seen in Figure 9.
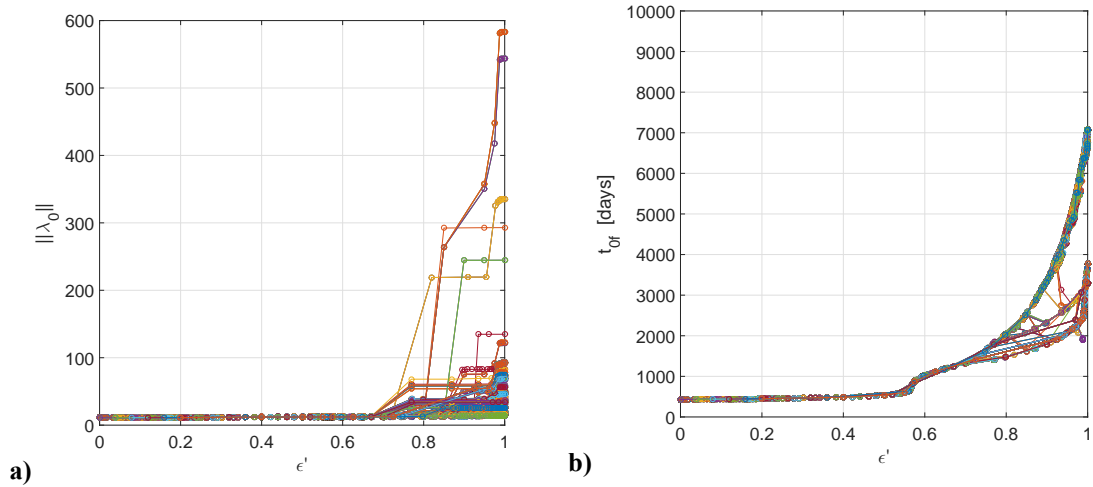

Figure 9. 2ⁿᵈ continuation zero-path branch solutions. In (a) the norm of the initial costates and in (b) the time of flight is plotted as function of the continuation parameter.

16

Both the zero-path components relative to the initial costates and the time of flight show several distinct branches leading to different final solutions at the end of the continuation, i.e. $\varepsilon' = 1$. Therefore multiple and distinct local minima have been found for the solar sail OCP with $a_c = 0.1$ mm/s^2. In particular, a better solution has been found with respect to the one shown in test case 4: the plots of the control and the transfer trajectory are shown in Figure 10. A summary of the results for the best solution found is provided in Table 6.
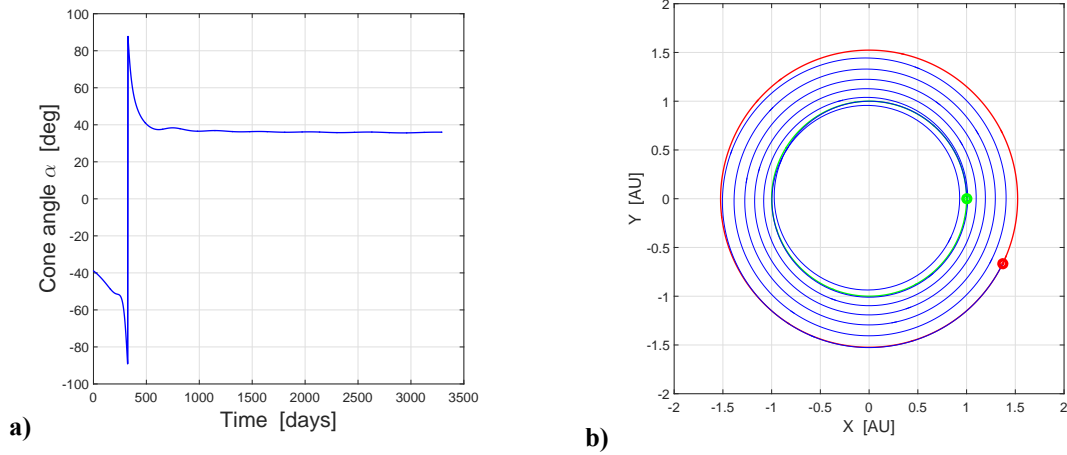

a)

b)

Figure 10. Best solution found, planar circular-to-circular Earth-Mars rendezvous with $a_c = 0.1$ mm/s^2. In (a) the cone angle evolution, in (b) the solar-sail transfer trajectory.

Table 6. Best solution found - planar circular-to-circular Earth-Mars rendezvous with $a_c = 0.1$ mm/s^2.

	Homotopy-continuation
Computational time [s]	30
t_{0f} [days]	3291.20

It is worth to note that in Figure 9 not all the branches converge at the end of the second continuation. In fact, it was found that for a limited number of branches the continuation stopped in proximity of the end. The authors believe that this issue is due to the numerical sensitivity of the discrete continuation algorithm to its operating parameters, that were altered in the analysis to discover the multiple zero-path solutions. However, manipulations carried on a sample set of not-converging branches demonstrated that convergent branching solutions could be obtained by suitably tuning the operating parameters of the discrete continuation algorithm.

It is also worth remarking that this analysis had the only purpose to discover and evince that multiple zero-path solutions do exist in the first and second homotopy. These zero-path solutions assume a branch nature in the second continuation, leading to different local minima in the case of solar-sail transfers with characteristic acceleration $a_c = 0.1$ mm/s^2. A further study, beyond the scope of this paper, should be carried on in order to properly detect the zero-path branches.

17

NUMERICAL STUDY OF LAUNCH DATES

A deeper investigation has led to determine an efficient way to compute the solar sail planet rendezvous OCP solutions for all the possible initial Earth-Mars phase displacements (Figure 11). This is essentially a proxy for all possible launch dates.
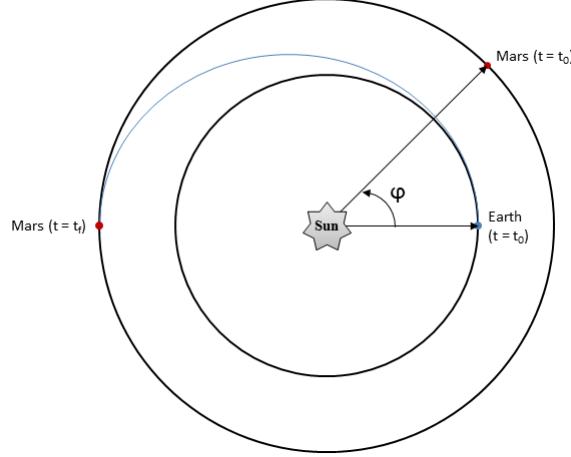

Figure 11. Illustration of the initial Earth-Mass phase displacement φ

The method makes use of a single initial low-thrust solution, which can be for an orbital transfer (numerically easier to compute) or for a planet rendezvous, with a certain initial Earth-Mars phase displacement $\varphi = \varphi_0$ ($\varphi_0 = 0 \deg$ in the case taken into account here). Subsequently, the solar-sail solution is computed by means of the homotopic approach and starting from the low-thrust one. Therefore, a discrete continuation on the initial phase displacement is performed, both forward and backward starting from $\varphi = \varphi_0$. The two continuations are respectively computed in the range $\varphi = [\varphi_0, \varphi_0 + 360 \deg]$ (forward) and $\varphi = [\varphi_0, \varphi_0 - 360 \deg]$ (backward); the solutions are obtained in steps of $\Delta\varphi = 10 \deg$. The forward and backward continuations allow detecting two different trends of the solar-sail planet-rendezvous optimal solutions, otherwise not noticeable with only one continuation.

In this study a solar sail with characteristic acceleration $a_c = 1 \, \mathrm{mm/s^2}$ has been considered. Figure 12a and Figure 12b plots the solar-sail minimum time of flight as function of the initial phase displacements, respectively in the range $\varphi \in [-360 \deg, +360 \deg]$ and in the range $\varphi \in [0 \deg, +360 \deg]$. The curves shows a minimum around $\varphi \approx 40 \deg$. The corresponding value is $t_{0f} = 412$ days. This is in line with the minimum time of flight found for the orbit transfer ($t_{0f} = 407$ days).
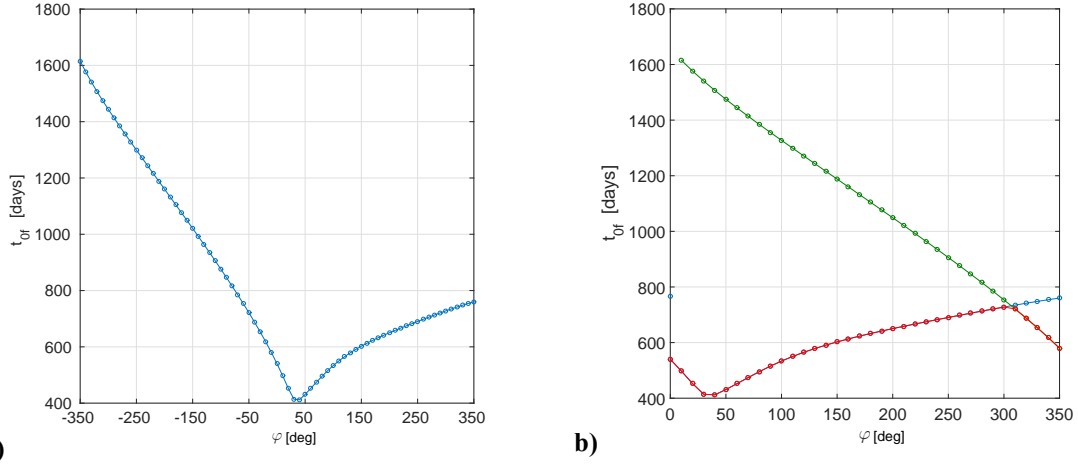
18

Figure 12. Solar-sail minimum time of flight as function of the initial relative phase displacement between Earth and Mars. (a) φ in [-360 deg, +360 deg]. (b) φ in [0 deg, +360 deg]. The lower curve in red represents the actual locus of the minimum time of flight solutions in the range [0 deg, +360 deg].

As visible in Figure 13, the two trends of the optimal solutions intersect between $\varphi = 300$ deg and $\varphi = 310$ deg. After this intersection, the OCP solutions of the ascending curve become as optimal as those ones of the descending curve. This corresponds to a change in the trend of the solar-sail optimal solution that can be immediately noticed by the shape of the solar-sail transfers across the intersection point, as shown in Figure 13. Ultimately, it is noteworthy to highlight that the computational time needed to get the full solar-sail planet-rendezvous solutions for all the initial phase displacements taken into account amounted to only 84 seconds.
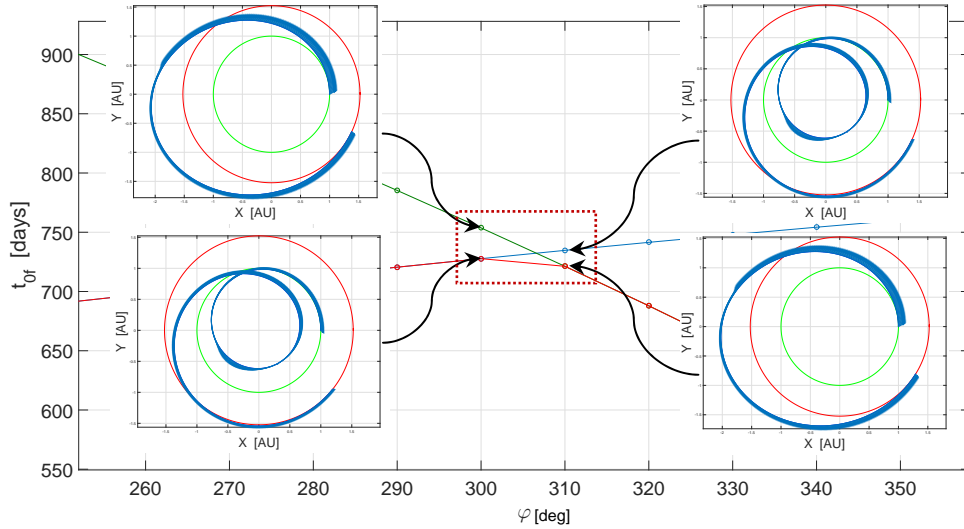

Figure 13. Zoom on the intersection point of the two curves in Figure 12b. The inlets show the type of transfers associated to each branch.

19

CONCLUSIONS

This paper presents a study using a homotopic and continuation approach to find minimum-time-of-flight solar-sail transfers starting from low-thrust ones. A solar-sail optimal control problem (OCP) solution is generally more difficult to compute respect to a low-thrust one due to the more restrictive dynamics constraints. This narrows the space of existence of feasible solutions in which the optimal ones are located. By adopting the homotopic approach, the authors demonstrated the efficiency of the novel technique in getting precise solar-sail OCP solutions in a short computational time. The strengths of the homotopic approach are especially noticeable in the solution of planet rendezvous problems, usually more difficult to compute respect to the simpler orbit rendezvous problems, and for any desired initial phase displacements between the departing and arriving planet. Given a low-thrust trajectory, in fact, one is able to easily and quickly find a solar-sail optimal trajectory; the genetic algorithm, instead, hardly finds solutions within the given tolerances, especially for planet rendezvous problems and with low characteristic acceleration. Moreover, the method allows having solar-sail solutions for a wide range of characteristic accelerations through a second continuation, which is performed on the characteristic acceleration itself. A deeper investigation has proven that branch-solutions exist in the zero-path of the homotopy. This leads to several local minima in the case of solar-sail transfers with low characteristic acceleration. This phenomenon motivates further studies focused on using more specific continuation algorithms that can efficiently and robustly detect bifurcation points in the zero-path of the homotopy and continue the branching solutions. The computation of the final solar-sail solutions for the branches found gives the possibility to detect and choose the best solution, in terms of time of flight, among the local minima.

REFERENCES

[1] Betts, J. T., *Practical Methods for Optimal Control and Estimation Using Nonlinear Programming (Second edition)*, 2010, pp. 91,123-126.

[2] Hull, D. G., *Optimal Control Theory for Applications*, New York, NY: Springer New York, 2003, pp. 11,12,293.

[3] Dachwald, B., and Seboldt, W., "Multiple near-Earth asteroid rendezvous and sample return using first generation solar sailcraft" *Acta Astronautica*, vol. 57, no. 11, 2005, pp. 864–875.

[4] Conway, B. A., *Spacecraft Trajectory Optimization*, Cambridge University Press 2010, 2010, pp. 1-7,16-36.

[5] Pontani, M., and Conway, B., "Optimal Low-Thrust Orbital Maneuvers via Indirect Swarming Method" *Journal of Optimization Theory and Applications*, vol. 162, no. 1, Nov. 2014, pp. 272–292.

[6] Pontani, M., and Conway, B. A., "Particle Swarm Optimization Applied to Space Trajectories" *Journal of Guidance, Control, and Dynamics*, vol. 33, no. 5, 2010, pp. 1429–1441.

[7] Whitehead, G. W., *Elements of Homotopy Theory*, New York, NY: Springer New York, 1978, pp. 3-8.

[8] Allgower, E. L., and Georg, K., "Introduction to Numerical Continuation Methods", *Classics in Applied Mathematics*, SIAM, vol. 45, 2003, pp. 1-6.

[9] Allgower, E. L., and Georg, K., "Numerical path following", *Handbook of numerical analysis*, P. G. Ciarlet and J. L. Lions, ed., North-Holland, 1997, pp. 5–7.

[10] Haberkorn, T., Martinon, P., and Gergaud, J., "Low Thrust Minimum-Fuel Orbital Transfer: A Homotopic Approach" *Journal of Guidance, Control, and Dynamics*, vol. 27, no. 6, 2004, pp. 1046–1060.

[11] Jiang, F., Baoyin, H., and Li, J., "Practical Techniques for Low-Thrust Trajectory Optimization with Homotopic Approach" *Journal of Guidance, Control, and Dynamics*, vol. 35, no. 1, Jan. 2012, pp. 245–258.

[12] Mengali, G., and Quarta, A. a., "Solar sail trajectories with piecewise-constant steering laws" *Aerospace Science and Technology*, vol. 13, no. 8, 2009, pp. 431–441.

[13] McInnes, C. R., *Solar Sailing: Technology, Dynamics and Mission Applications*, Springer Praxis Publishing, 1999, pp. 115-116.

[14] More, J. J., "The Levenberg-Marquardt algorithm: Implementation and theory" *Lecture Notes in Mathematics*, vol. 630, no. x, 1978, pp. 105–116.

[15] Stoer, J., and Bulirsch, R., *Introduction to Numerical Analysis*, New York, NY: Springer New York, 2002, pp. 521-524.

[16] Strogatz, S. H., *Nonlinear Dynamics and Chaos*, Westview Press, 1994, pp. 44-45,241.

[17] Doedel, E., Keller, H. B., and Kernevez, J. P., "Numerical Analysis and Control of Bifurcation Problems (I): Bifurcation in Finite Dimensions" *International Journal of Bifurcation and Chaos*, vol. 01, no. 3, 1991, pp. 493–520.